Nonlinear Dyn (2018) 92:2159–2175
https://doi.org/10.1007/s11071-018-4187-0

ORIGINAL PAPER

Dynamic analysis of integrally shrouded group blades with rubbing and impact

Bingbing He · Huajiang Ouyang · Shangwen He · Xingmin Ren · Yonggang Mei

Received: 18 May 2017 / Accepted: 4 March 2018 / Published online: 29 March 2018

Abstract Forced vibration responses of integrally shrouded group blades are investigated in this paper. A lumped mass model of integrally shrouded group blades considering centrifugal stiffening of the blade and rubbing and impact between adjacent shrouds is established. In the proposed model, collision force is approximated by linear springs, and friction force is approximated by an exponential-type velocity-dependent model. Stick-slip-separation transition boundaries are determined. Runge–Kutta algorithm is used to compute vibration responses and study the effects of stiffness ratio, rotating speed and aerodynamic excitation amplitude on the vibration responses of integrally shrouded group blades. Vibration reduction effect of the shroud on the reference blade at the first dynamic resonance speed is illustrated. Numerical results indicate that stiffness ratio, initial gap and contact angle have a great effect on the normalised energy density (the value of which can represent vibration reduction effect of the shroud), and the reference blade can experience periodic, quasi-periodic and chaotic vibration due to nonsmooth behaviour at the shroud contact interfaces.

Keywords Integrally shrouded blade · Rubbing-impact · Friction · Nonlinear vibration · Nonsmooth · Energy dissipation

B. He · X. Ren
School of Mechanics, Civil Engineering and Architecture, Northwestern Polytechnical University, Xi'an 710072, China
e-mail: hebb714@gmail.com

H. Ouyang (✉)
State key Laboratory of Structural Analysis for Industrial Equipment, Dalian University of Technology, Dalian 116023, China
e-mail: huajiang.ouyang@gmail.com

H. Ouyang
School of Engineering, University of Liverpool, Liverpool L69 3GH, England, UK

S. He
School of Mechanics & Engineering Science, Zhengzhou University, Zhengzhou 450001, China
e-mail: hsw2013@zzu.edu.cn

Y. Mei
School of Mechanical Engineering, Northwestern Polytechnical University, Xi'an 710072, China
e-mail: meiyonggang@mail.nwpu.edu.cn

1 Introduction

Blades are major components in aeroengines. High-cycle fatigue (HCF) failure due to high dynamic stresses caused by blade vibration is one of the main causes of aeroengine incidents [1–3]. A shroud device of the blade is actually an effective dry friction damper to reduce vibration amplitudes and high dynamic stresses of turbine blades, thus, it is widely used as a means of vibration suppression for turbine blades. The contact interfaces of adjacent blade shrouds may undergo stick and slip, and separation, and the contact force may possess nonlinear characteristics. These lead to many difficulties to predict its dynamic response accurately.

Extensive research into nonlinear behaviour of the integrally shrouded blade has been conducted. Nonlinear dynamic model of shrouded group blades considering contact and impact based on Hertz contact force theory was built in [4]. A three-dimensional finite element model for vibration analysis of group blades was presented in [5]. The model improved the accuracy for calculating the natural frequencies and mode shapes of group blades, and offered an effective way for calculating vibratory modes of integral blades with complex shapes. The influence on coupled vibrations of shaft-torsion and blade-bending of a rotor system with grouped blades was studied by Chiu et al. [6] analytically. The rotating vibration behaviour of a full circle of the turbine blades with different groups of blades was investigated in [7]. A macro-slip model of a single point contact which assumes that all points on the contact interface are sticking or slipping all at the same time is widely used in many investigations [8–11]. The famous bilinear hysteretic restoring force model was put forward by Iwan [12]. Hao and Zhu [13] applied the hysteresis spring model to a two-dimensional contact friction analysis and introduced a dynamic compliance method to resolve the response of complex structures with dry friction. Yang and Menq [14] developed a three-dimensional friction contact model for the prediction of the resonant response of structures having three-dimensional frictional constraints. A numerical method was introduced to calculate the nonlinear friction force by tracing the trajectory of the relative motion of the moving contact point when friction interface was constrained to complex contact motions [15]. The forced response of a blade with shrouds of a low pressure steam turbine was computed and numerical results were compared with the experimental results of Wheel Box Tests performed at GE Oil & Gas [16]. A reduced order model (ROM) was proposed based on an appropriate nonlinear modal basis, and the methodology was applied to both a simplified and a large-scale model of a bladed disc with shroud contact interfaces [17]. Experimental modelling and numerical simulation of blade interaction by means of a friction element placed in the shroud between the blade heads were carried out in [18]. By dividing a complete stick-slip cycle of the damper into four intervals in succession, Ding and Chen [19] proposed an analytical method for determining the steady-state response of a blade with dry friction. Sgn contact model was used to study the dynamic response of a two-degree of freedom lumped mass model of a shrouded blade, and effects of some parameters on nonlinear dynamic characteristics of the system were analysed [20].

Iwan [21] presented a parallel-series model and a series-parallel model based on the assumption that there was partial sliding at the contact interface. A continuous microslip model of friction which allowed partial slipping at the friction interface in elastoplastic shear layer theory was presented by Menq et al. [22,23] a few years later. In some cases, when there is coupling between motions of a structure in more than one direction, a one-dimensional motion model is not valid. A two-dimensional microslip friction model was proposed in [24], then Cigeroglu et al. [25] put forward a two-dimensional distributed parameter microslip friction model with normal load variation induced by normal motion which characterised the stick-slip-separation of the contact interface.

For the study of the impact force, Freudenstein [26] proposed an impact pair model. Chu et al. [27] approximated collision force by linear springs in their investigation. Nan [28] established a shrouded blade model composed of springs and a cantilever beam with a tip mass, and the effects of the stiffness ratio, the mass ratio and the amplitude of the excitation on vibration of the system were analysed. How the number of blades and distribution of cracks affected the mode localisation of a mistuned blade system was examined in [29]. A modelling method for a flexible beam with a tip mass that experienced impact, while undergoing large overall motion was presented in [30]. A recent experimental technique and damping reduction method for isolating the structural damping of rotating blades was demonstrated by Jeffers et al. [31]. Ma et al. [32] established a dynamic model of rotating shrouded blades considering the effects of the centrifugal stiffening, spin softening and Coriolis force. It was found in [27] that contact stiffness had very important effects on the impact force between adjacent shrouded blades. A friction contact stiffness model of fractal geometry was proposed to investigate the nonlinear vibration behaviour of a shrouded blade [33]. Multi-harmonic balance method (MHBM) was used to obtain the steady-state periodic solutions of shrouded turbine blade systems [34,35]. The gap between adjacent shrouds and the rotating speed of the blade disc were found to have significant effects on the dynamical responses of the system [36].

Although much work has been done on the vibration analysis of integrally shrouded blades, most studies

only consider impact between neighbouring shrouds, and rubbing existing between adjacent shrouds has not been included. A more realistic model which accommodates rubbing impact and can deal with stick-slip-separation of the contact interfaces and thus possesses nonlinear characteristics of the contact force is needed. In this paper, a lumped mass model of integrally shrouded group blades is established, and centrifugal stiffening of the blades, and rubbing and impact between adjacent shrouds are considered. Impact force is modelled by linear springs. An exponential-type velocity-dependent friction model which is commonly used for contact between solid surfaces in dry conditions is adopted to describe the friction force. Equations of motion of the integrally shrouded group blades in different dynamic situations are derived, and stick-slip-separation transition boundaries are determined. A numerical approach for solving the forced vibration of integrally shrouded group blades with impact and non-smooth friction contact is presented.

2 Mechanical model and dynamics equations of integrally shrouded group blades

The whole group of integrally shrouded blades forms a circular structure. In order to study the influence of collision force and friction force to the vibration characteristics of shrouded blades, a set of three blades are taken in this study. It is assumed that the disc is rigid, while the blades are elastic in this investigation. The schematic of integrally shrouded group blades of an aeroengine is shown in Fig. 1, where the xyz coordinate system (called the global cylindrical coordinate system) is defined in accordance with the tangential (x), radial (y), and axial (z) directions.

Actually, the contact-rubbing between the adjacent shrouds takes place in three perpendicular directions. However, the main direction of aerodynamic excitation force is in the rotating tangential direction of bladed disc (x), and the blades are easy to bend in this direction. In addition, the displacements in the y and z directions are very small in relation to the displacement in the x direction, thus can be ignored. In this paper, centrifugal stiffening is considered. ANSYS is used to get the frequencies of the shrouded blade considering the pre-stress effects (produced by the centrifugal force due to rotation of the turbine disc in an aeroengine). First, the pre-stress of the shrouded blade under rotating condition is acquired, and then, its frequencies including pre-stress effects are obtained. The first natural frequency $f_{\mathrm{d}1}$ at various rotating disc speeds is obtained from the FE model and can be fitted into a curve shown in Fig. 2. Then, its dynamic stiffness can be obtained.

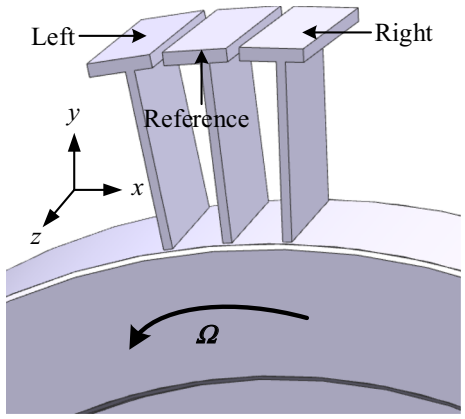

Fig. 1 The schematic of integrally shrouded group blades of an aeroengine

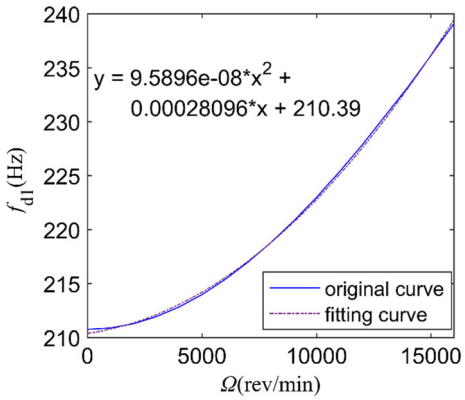

Fig. 2 First dynamic frequency versus rotating speed curve and its fitting curve

The integrally shrouded group blades are simplified as a lumped mass model each, as shown in Fig. 3. Accordingly, the equations of motion could be written as

$$\begin{aligned}
&m_1\ddot{x}_1 + c_1\dot{x}_1 + k_1x_1 = Q_1 - F_1\left(t, x_1 - x_2, \dot{x}_1 - \dot{x}_2, \Delta_1\right)\\
&m_2\ddot{x}_2 + c_2\dot{x}_2 + k_2x_2 = Q_2 + F_1\left(t, x_1 - x_2, \dot{x}_1 - \dot{x}_2, \Delta_1\right)\\
&\qquad - F_2\left(t, x_2 - x_3, \dot{x}_2 - \dot{x}_3, \Delta_2\right)\\
&m_3\ddot{x}_3 + c_3\dot{x}_3 + k_3x_3 = Q_3 + F_2\left(t, x_2 - x_3, \dot{x}_2 - \dot{x}_3, \Delta_2\right)
\end{aligned} \tag{1}$$

Q_1, Q_2 and Q_3 are aerodynamic excitation forces acting on the three masses, the frequency of the excita-

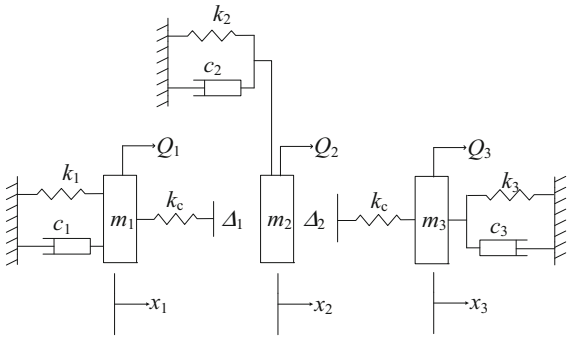

Fig. 3 Mechanical model of integrally shrouded group blades

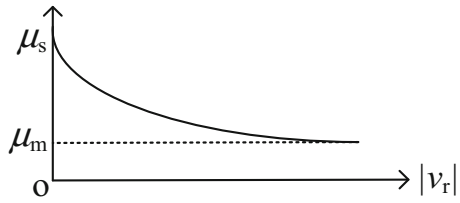

Fig. 5 An exponential-type friction coefficient versus relative velocity curve

tion f_e is l times of the rotating frequency f_r of the blade, where l is the number of obstacles in the front of the rotor-blade [27]. $Q_i = q_0 + q_1 \sin(l\Omega t + \varphi_i) + q_2 \sin(2l\Omega t + \varphi_i) + \cdots + q_n \sin(nl\Omega t + \varphi_i)$, $i = 1, 2, 3$; q_0 is a time-independent constant force, q_n is the amplitude of the n-th harmonic component, $(n = 1, 2, 3 \ldots)$. F_1 and F_2 are the nonlinear forces between integrally shrouded group blades with rub and impact. Δ_1 and Δ_2 are the initial gaps between the adjacent blade shrouds when they are stationary. Ω is the rotating angular velocity of the disc. In this paper, only the first harmonic component of aerodynamic excitation is adopted (namely, excitation terms above q_1 are excluded, as commonly done); it is taken that $l = 2$ and $f_e = 2f_r$. The phase difference between neighbouring blades was found to play an important role, and the best damping effect was obtained in the case of an anti-phase vibration mode [9]. Thus it is assumed that the phase difference should be $\varphi_2 - \varphi_1 = \pi$, $\varphi_3 - \varphi_2 = \pi$.

During engine operation, rub-impact between adjacent blade shrouds is very complicated, normal motion of the contact surfaces could bring about variation of the collision force and separation of the contact surfaces, and the contact interface may experience stick or slip motion due to the relative tangential motion of the contact surfaces. The geometrical relations of the displacements and forces on the contact interface is displayed in Fig. 4.

Collision between adjacent shrouds is assumed to be a single point elastic collision which should be completed in a certain period of time, the whole process including four stages: contact, compression deformation, recovery and separation. The normal force N_1 and N_2 imposed on the shroud of the blade are described as [37]

$$N_1 = \begin{cases} k_c (x_1 - x_2 - \Delta_1) \sin\alpha & x_1 - x_2 > \Delta_1 \\ 0 & x_1 - x_2 \le \Delta_1 \end{cases} \quad (2)$$

$$N_2 = \begin{cases} k_c (x_2 - x_3 - \Delta_2) \sin\alpha & x_2 - x_3 > \Delta_2 \\ 0 & x_2 - x_3 \le \Delta_2 \end{cases} \quad (3)$$

where k_c is the elastic coefficient between the contact surfaces, α is the contact angle. An exponential-type velocity-dependent friction model is considered in the present study. Friction force asymptotically decreases as the relative velocity increases (Fig. 5). This type of

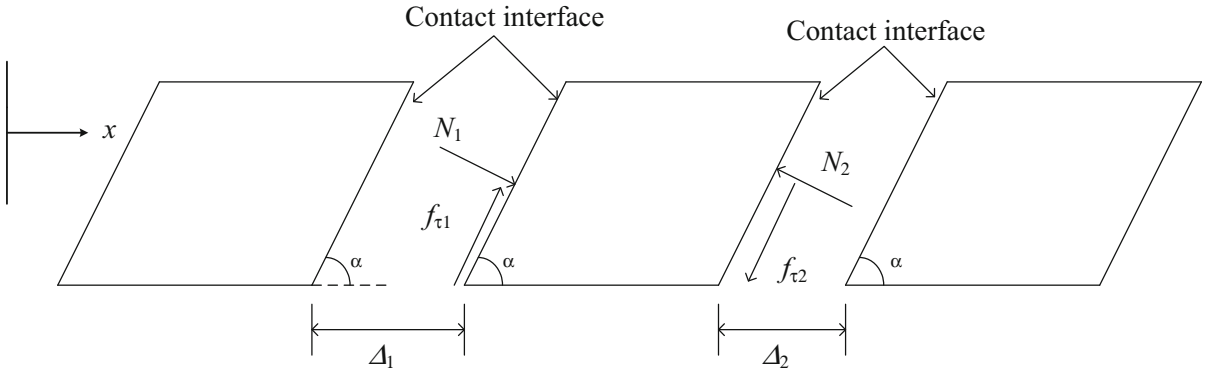

Fig. 4 The geometrical relations of the displacements and forces on the contact interface

friction model is commonly used for contact between solid surfaces in dry conditions, and its coefficient function (as introduced in [38]) can be expressed as

$$\mu\left(v_{\mathrm{r}}\right)=\mu_{\mathrm{m}}+\left(\mu_{\mathrm{s}}-\mu_{\mathrm{m}}\right)\mathrm{e}^{-\beta\left|v_{\mathrm{r}}\right|} \tag{4}$$

where μ_{m} is the minimum kinetic friction coefficient, μ_{s} is the maximum static friction coefficient, β is a tuning parameter used to control the negative slope of the friction coefficient curve, v_{r} is the relative velocity between contact surfaces of adjacent shrouds: $v_{\mathrm{r}1}=(\dot{x}_1-\dot{x}_2)\cos\alpha$, $v_{\mathrm{r}2}=(\dot{x}_2-\dot{x}_3)\cos\alpha$.

Friction forces $f_{\tau 1}$ and $f_{\tau 2}$ governed by the classical Coulomb's law of friction can be written as

$$f_{\tau 1}=\begin{cases}\mu\left(v_{\mathrm{r}1}\right)N_1\mathrm{sgn}\left(v_{\mathrm{r}1}\right) & v_{\mathrm{r}1}\neq 0\\ -\mu_{\mathrm{s}}N_1\leq f_{\tau 1}\leq\mu_{\mathrm{s}}N_1 & v_{\mathrm{r}1}=0\end{cases} \tag{5}$$

$$f_{\tau 2}=\begin{cases}\mu\left(v_{\mathrm{r}2}\right)N_2\mathrm{sgn}\left(v_{\mathrm{r}2}\right) & v_{\mathrm{r}2}\neq 0\\ -\mu_{\mathrm{s}}N_2\leq f_{\tau 2}\leq\mu_{\mathrm{s}}N_2 & v_{\mathrm{r}2}=0\end{cases} \tag{6}$$

According to Fig. 4 and Eqs. (2–6), Eq. (1) can be rewritten as

$$\begin{aligned}&m_1\ddot{x}_1+c_1\dot{x}_1+k_1x_1=Q_1-N_1\sin\alpha-f_{\tau 1}\cos\alpha\\&m_2\ddot{x}_2+c_2\dot{x}_2+k_2x_2=Q_2+N_1\sin\alpha\\&\quad+f_{\tau 1}\cos\alpha-N_2\sin\alpha-f_{\tau 2}\cos\alpha\\&m_3\ddot{x}_3+c_3\dot{x}_3+k_3x_3=Q_3+N_2\sin\alpha+f_{\tau 2}\cos\alpha\end{aligned} \tag{7}$$

Select $m_1=m_2=m_3=m$, $c_1=c_2=c_3=c$ and $k_1=k_2=k_3=k$. Denote $\omega^2=\frac{k}{m}$, $\varepsilon=\frac{c}{2m\omega}$, $\eta=\frac{\Omega}{\omega}$, $K=\frac{\Delta_2}{\Delta_1}$, $X_1=\frac{x_1}{\Delta_1}$, $X_2=\frac{x_2}{\Delta_1}$, $X_3=\frac{x_3}{\Delta_1}$, $\tau=\omega t$, $(*)'=\frac{\mathrm{d}*}{\mathrm{d}\tau}$, $\gamma_1=\frac{k_{\mathrm{c}}}{k}$, $\bar{Q}_1=\frac{Q_1}{m\Delta_1\omega^2}$, $\bar{Q}_2=\frac{Q_2}{m\Delta_1\omega^2}$, $\bar{Q}_3=\frac{Q_3}{m\Delta_1\omega^2}$, $\bar{f}_{\tau 1}=\frac{f_{\tau 1}}{m\Delta_1\omega^2}$, $\bar{f}_{\tau 2}=\frac{f_{\tau 2}}{m\Delta_1\omega^2}$, $X_{\mathrm{r}1}=X_1-X_2-1$, $X_{\mathrm{r}2}=X_2-X_3-K$, $\bar{N}_1=\frac{N_1}{m\Delta_1\omega^2}$, $\bar{N}_2=\frac{N_2}{m\Delta_1\omega^2}$, $\bar{N}=\bar{N}_1-\bar{N}_2$, $\bar{f}_\tau=\bar{f}_{\tau 1}-\bar{f}_{\tau 2}$, $\bar{v}_{\mathrm{r}1}=X'_{\mathrm{r}1}\cos\alpha$,$\bar{v}_{\mathrm{r}2}=X'_{\mathrm{r}2}\cos\alpha$. Doing these will simplify the mathematical expressions of Eq. (7).

There are four kinds of contact states between the reference shroud and its left- and right-side shrouds:

1. There is no contact between the reference shroud and its left- and right-side shrouds, thus, $X_{\mathrm{r}1}\leq 0$ and $X_{\mathrm{r}2}\leq 0$, $\bar{N}_1=0$, $\bar{N}_2=0$, $\bar{f}_{\tau 1}=0$, $\bar{f}_{\tau 2}=0$, and Eq. (7) is simplified to the dimensionless equation as

$$\begin{aligned}&X''_1+2\varepsilon X'_1+X_1=\bar{Q}_1\\&X''_2+2\varepsilon X'_2+X_2=\bar{Q}_2\\&X''_3+2\varepsilon X'_3+X_3=\bar{Q}_3\end{aligned} \tag{8}$$

2. There is contact only between the reference shroud and its left-side shroud, thus, $X_{\mathrm{r}1}>0$ and $X_{\mathrm{r}2}\leq 0$. Three scenarios can happen as follows.

(a) If the reference shroud is slipping relatively to the left shroud, $X'_{\mathrm{r}1}\neq 0$. $\bar{f}_{\tau 1}=\mu\left(\bar{v}_{\mathrm{r}1}\right)\bar{N}_1\mathrm{sgn}\left(\bar{v}_{\mathrm{r}1}\right)$ is the dimensionless sliding friction force, where $\bar{N}_1=\gamma_1X_{\mathrm{r}1}\sin\alpha$. Because there is no contact between the reference shroud and the right shroud, $\bar{N}_2=0$, $\bar{f}_{\tau 2}=0$. Therefore, Eq. (7) is simplified to the dimensionless equation as

$$\begin{aligned}&X''_1+2\varepsilon X'_1+X_1=\bar{Q}_1\\&\quad-\bar{N}_1\left[\sin\alpha+\mu\left(\bar{v}_{\mathrm{r}1}\right)\cos\alpha\mathrm{sgn}\left(\bar{v}_{\mathrm{r}1}\right)\right]\\&X''_2+2\varepsilon X'_2+X_2=\bar{Q}_2\\&\quad+\bar{N}_1\left[\sin\alpha+\mu\left(\bar{v}_{\mathrm{r}1}\right)\cos\alpha\mathrm{sgn}\left(\bar{v}_{\mathrm{r}1}\right)\right]\\&X''_3+2\varepsilon X'_3+X_3=\bar{Q}_3\end{aligned} \tag{9}$$

(b) If the reference shroud is sticking relatively to the left shroud, $X'_{\mathrm{r}1}=0$ and $|\bar{f}_{\tau 1}|\leq\mu_{\mathrm{s}}\bar{N}_1$, where $\bar{f}_{\tau 1}$ is the dimensionless static friction force at this time; $X_1-X_2=\mathrm{C}_1$, $X'_1=X'_2$, where C_1 is the horizontal displacement difference between the left shroud and the reference shroud at the end of the previous slip phase; Equation (7) is now simplified to the dimensionless equation as

$$\begin{aligned}&X''_1+2\varepsilon X'_1+X_1=\frac{1}{2}\left(\bar{Q}_1+\bar{Q}_2+\mathrm{C}_1\right)\\&X''_2+2\varepsilon X'_2+X_2=\frac{1}{2}\left(\bar{Q}_1+\bar{Q}_2-\mathrm{C}_1\right)\\&X''_3+2\varepsilon X'_3+X_3=\bar{Q}_3\end{aligned} \tag{10}$$

The first row of Eq. (7) minus the second row of Eq. (7) can be simplified to a dimensionless equation as $X''_1-X''_2+2\varepsilon X'_1-2\varepsilon X'_2+X_1-X_2=\bar{Q}_1-\bar{Q}_2-2\bar{N}_1\sin\alpha-2\bar{f}_{\tau 1}\cos\alpha$, due to $X_1-X_2=\mathrm{C}_1$, $X'_1=X'_2$, $X''_1=X''_2$, thus, $\mathrm{C}_1=\bar{Q}_1-\bar{Q}_2-2\bar{N}_1\sin\alpha-2\bar{f}_{\tau 1}\cos\alpha$, so the dimensionless static friction force $\bar{f}_{\tau 1}$ can be written as

$$\bar{f}_{\tau 1}=\frac{-1}{2\cos\alpha}\left(\bar{Q}_2-\bar{Q}_1+2\bar{N}_1\sin\alpha+\mathrm{C}_1\right) \tag{11}$$

(c) If $X'_{\mathrm{r}1}=0$ and $|\bar{f}_{\tau 1}|>\mu_{\mathrm{s}}\bar{N}_1$ ($\bar{f}_{\tau 1}$ can be obtained from Eq. (11)), friction force reverses its direction, the reference shroud and the left-side shroud is still in sliding state.

3. If the reference shroud is in contact with the right-side shroud but without contact with the left-side shroud, therefore, $X_{r2} > 0$ and $X_{r1} \leq 0$. Again three scenarios can happen as follows.

(a) If the reference shroud is slipping relatively to the right-side shroud, $X'_{r2} \neq 0$, $\bar{f}_{\tau 2} = \mu(\bar{v}_{r2})\bar{N}_2 \mathrm{sgn}(\bar{v}_{r2})$ is the dimensionless sliding friction force, where $\bar{N}_2 = \gamma_1 X_{r2} \sin\alpha$. As there is no contact between the reference and the left-side shrouds, $\bar{N}_1 = 0$, $\bar{f}_{\tau 1} = 0$. Equation (7) is simplified to the dimensionless equation as

$$\begin{aligned} &X''_1 + 2\varepsilon X'_1 + X_1 = \bar{Q}_1 \\ &X''_2 + 2\varepsilon X'_2 + X_2 = \bar{Q}_2 \\ &\quad - \bar{N}_2\left[\sin\alpha + \mu(\bar{v}_{r2})\cos\alpha \mathrm{sgn}(\bar{v}_{r2})\right] \\ &X''_3 + 2\varepsilon X'_3 + X_3 = \bar{Q}_3 \\ &\quad + \bar{N}_2\left[\sin\alpha + \mu(\bar{v}_{r2})\cos\alpha \mathrm{sgn}(\bar{v}_{r2})\right] \end{aligned} \tag{12}$$

(b) If the reference shroud is sticking relatively to the right-side shroud, $X'_{r2} = 0$ and $|\bar{f}_{\tau 2}| \leq \mu_s \bar{N}_2$, $\bar{f}_{\tau 2}$ is the dimensionless static friction force, $X_2 - X_3 = C_2$, $X''_2 = X''_3$, C_2 is the horizontal displacement difference between the reference shroud and the right shroud at the end of the previous slip phase; Equation (7) is simplified to the dimensionless equation as

$$\begin{aligned} &X''_1 + 2\varepsilon X'_1 + X_1 = \bar{Q}_1 \\ &X''_2 + 2\varepsilon X'_2 + X_2 = \frac{1}{2}\left(\bar{Q}_2 + \bar{Q}_3 + C_2\right) \\ &X''_3 + 2\varepsilon X'_3 + X_3 = \frac{1}{2}\left(\bar{Q}_2 + \bar{Q}_3 - C_2\right) \end{aligned} \tag{13}$$

The second row of Eq. (7) minus the third row of Eq. (7) can be simplified to a dimensionless equation as $X''_2 - X''_3 + 2\varepsilon X'_2 - 2\varepsilon X'_3 + X_2 - X_3 = \bar{Q}_2 - \bar{Q}_3 - 2\bar{N}_2 \sin\alpha - 2\bar{f}_{\tau 2}\cos\alpha$, due to $X_2 - X_3 = C_2$, $X'_2 = X'_3$, $X''_2 = X''_3$, thus, $C_2 = \bar{Q}_2 - \bar{Q}_3 - 2\bar{N}_2 \sin\alpha - 2\bar{f}_{\tau 2}\cos\alpha$, so the dimensionless static friction force $\bar{f}_{\tau 2}$ can be written as

$$\bar{f}_{\tau 2} = \frac{-1}{2\cos\alpha}\left(\bar{Q}_3 - \bar{Q}_2 + 2\bar{N}_2 \sin\alpha + C_2\right) \tag{14}$$

(c) If $X'_{r2} = 0$ and $|\bar{f}_{\tau 2}| > \mu_s \bar{N}_2$ ($\bar{f}_{\tau 2}$ can be obtained from Eq. (14)), friction force reverses its direction, and the reference shroud and the right-side shroud is still in sliding state.

4. There are contacts between the reference shroud and the left- and right-side shrouds, hence, $X_{r1} > 0$ and $X_{r2} > 0$, $\bar{N}_1 = \gamma_1 X_{r1} \sin\alpha$, $\bar{N}_2 = \gamma_1 X_{r2} \sin\alpha$. There are four kinds of motion states in this situation.

(a) The reference shroud is slipping relatively to the left- and right-side shrouds, and Eq. (7) is simplified to the dimensionless equation as

$$\begin{aligned} &X''_1 + 2\varepsilon X'_1 + X_1 = \bar{Q}_1 \\ &\quad - \bar{N}_1\left[\sin\alpha + \mu(\bar{v}_{r1})\cos\alpha \mathrm{sgn}(\bar{v}_{r1})\right] \\ &X''_2 + 2\varepsilon X'_2 + X_2 = \bar{Q}_2 \\ &\quad + \bar{N}_1\left[\sin\alpha + \mu(\bar{v}_{r1})\cos\alpha \mathrm{sgn}(\bar{v}_{r1})\right] \\ &\quad - \bar{N}_2\left[\sin\alpha + \mu(\bar{v}_{r2})\cos\alpha \mathrm{sgn}(\bar{v}_{r2})\right] \\ &X''_3 + 2\varepsilon X'_3 + X_3 = \bar{Q}_3 \\ &\quad + \bar{N}_2\left[\sin\alpha + \mu(\bar{v}_{r2})\cos\alpha \mathrm{sgn}(\bar{v}_{r2})\right] \end{aligned} \tag{15}$$

(b) The reference shroud is slipping relatively to the left-side shroud but sticking relatively to the right-side shroud, and Eq. (7) is simplified to the dimensionless equation as

$$\begin{aligned} &X''_1 + 2\varepsilon X'_1 + X_1 = \bar{Q}_1 \\ &\quad - \bar{N}_1\left[\sin\alpha + \mu(\bar{v}_{r1})\cos\alpha \mathrm{sgn}(\bar{v}_{r1})\right] \\ &X''_2 + 2\varepsilon X'_2 + X_2 = \frac{1}{2}\left\{\bar{Q}_2 + \bar{N}_1\left[\sin\alpha\right.\right. \\ &\quad \left.\left. + \mu(\bar{v}_{r1})\cos\alpha \mathrm{sgn}(\bar{v}_{r1})\right] + \bar{Q}_3 + C_2\right\} \\ &X''_3 + 2\varepsilon X'_3 + X_3 = \frac{1}{2}\left\{\bar{Q}_2 + \bar{N}_1\left[\sin\alpha\right.\right. \\ &\quad \left.\left. + \mu(\bar{v}_{r1})\cos\alpha \mathrm{sgn}(\bar{v}_{r1})\right] + \bar{Q}_3 - C_2\right\} \end{aligned} \tag{16}$$

At this moment, the dimensionless static friction force can be written as

$$\begin{aligned} \bar{f}_{\tau 2} = \frac{-1}{2\cos\alpha}&\left\{\bar{Q}_3 - \bar{Q}_2 - \bar{N}_1\left[\sin\alpha\right.\right. \\ &\left.\left. + \mu(\bar{v}_{r1})\cos\alpha \mathrm{sgn}(\bar{v}_{r1})\right] + 2\bar{N}_2 \sin\alpha + C_2\right\} \end{aligned} \tag{17}$$

(c) The reference shroud is slipping relative to the right-side shroud but sticking relative to the left-side shroud, and Eq. (6) is simplified to the dimensionless equation as

$$\begin{aligned} &X''_1 + 2\varepsilon X'_1 + X_1 = \frac{1}{2}\left\{\bar{Q}_1 + \bar{Q}_2\right. \\ &\quad \left. - \bar{N}_2\left[\sin\alpha + \mu(\bar{v}_{r2})\cos\alpha \mathrm{sgn}(\bar{v}_{r2})\right] + C_1\right\} \\ &X''_2 + 2\varepsilon X'_2 + X_2 = \frac{1}{2}\left\{\bar{Q}_1\right. \end{aligned}$$

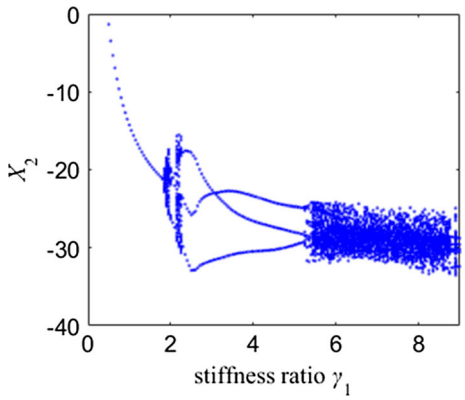

Fig. 6 Bifurcation diagram of the reference blade versus stiffness ratio γ_1 ($\Omega = 6000\,\mathrm{rev/min}$, $q_1 = 50\,\mathrm{N}$)

$$+\bar{Q}_2-\bar{N}_2\left[\sin\alpha+\mu\left(\bar{v}_{r2}\right)\cos\alpha\,\mathrm{sgn}\left(\bar{v}_{r2}\right)\right]-\mathrm{C}_1\Big\}$$
$$X_3''+2\varepsilon X_3'+X_3=\bar{Q}_3$$
$$+\bar{N}_2\left[\sin\alpha+\mu\left(\bar{v}_{r2}\right)\cos\alpha\,\mathrm{sgn}\left(\bar{v}_{r2}\right)\right] \quad (18)$$

At this time, the dimensionless static friction force $\bar{f}_{\tau 1}$ can be written as

$$\bar{f}_{\tau 1}=\frac{-1}{2\cos\alpha}\left(\bar{Q}_2-\bar{N}_2\left[\sin\alpha+\mu\left(\bar{v}_{r2}\right)\cos\alpha\right.\right.$$
$$\left.\left.\times\mathrm{sgn}\left(\bar{v}_{r2}\right)\right]-\bar{Q}_1+2\bar{N}_1\sin\alpha+\mathrm{C}_1\right) \quad (19)$$

(d) The reference shroud is sticking relative to the left- and right-side shrouds, and Eq. (7) is simplified to the dimensionless equation as

$$X_1''+2\varepsilon X_1'+X_1=\frac{1}{3}\left(\bar{Q}_1+\bar{Q}_2\right.$$
$$\left.+\bar{Q}_3+2\mathrm{C}_1+\mathrm{C}_2\right)$$
$$X_2''+2\varepsilon X_2'+X_2=\frac{1}{3}\left(\bar{Q}_1+\bar{Q}_2\right.$$
$$\left.+\bar{Q}_3-\mathrm{C}_1+\mathrm{C}_2\right)$$
$$X_3''+2\varepsilon X_3'+X_3=\frac{1}{3}\left(\bar{Q}_1+\bar{Q}_2\right.$$
$$\left.+\bar{Q}_3-\mathrm{C}_1-2\mathrm{C}_2\right) \quad (20)$$

The dimensionless static friction force $\bar{f}_{\tau 1}$ and $\bar{f}_{\tau 2}$ can be, respectively, described as

$$\bar{f}_{\tau 1}=\frac{-1}{3\cos\alpha}\left(\bar{Q}_2+\bar{Q}_3-2\bar{Q}_1\right.$$
$$\left.+3\bar{N}_1\sin\alpha+2\mathrm{C}_1+\mathrm{C}_2\right) \quad (21)$$

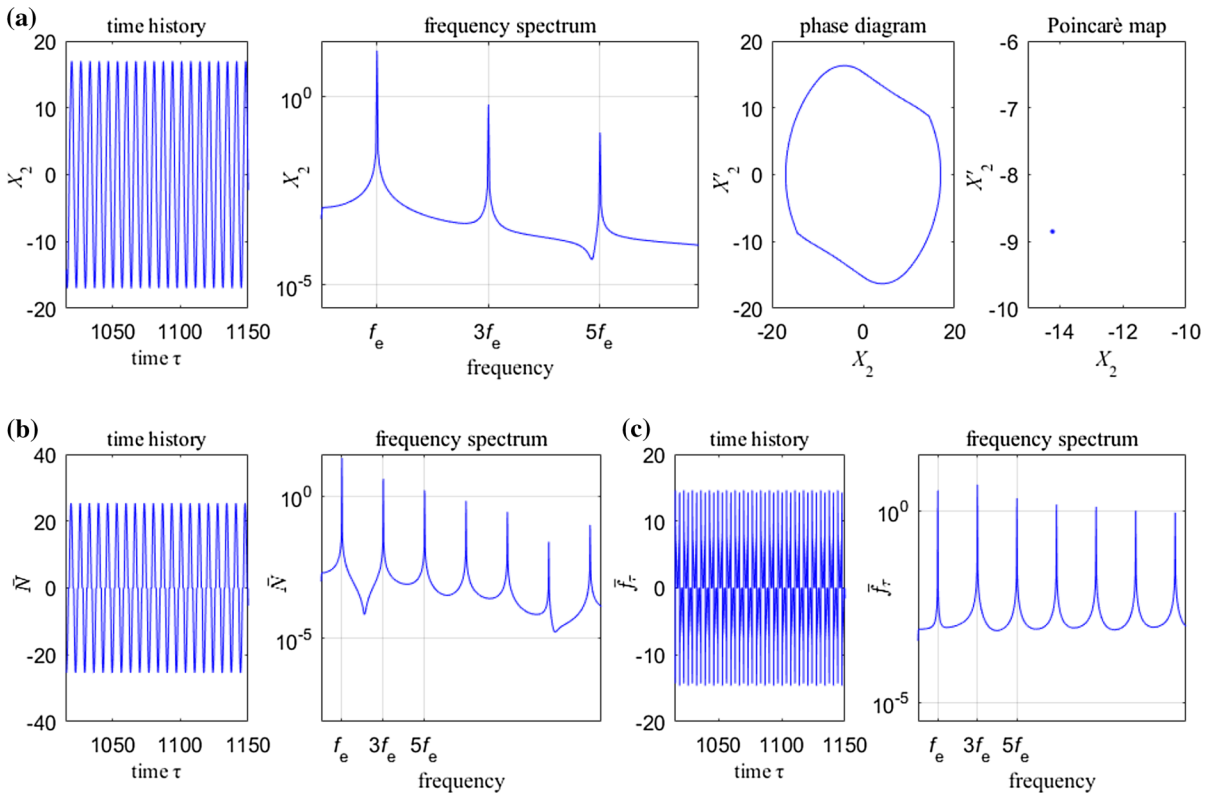

Fig. 7 Vibration responses of the reference blade ($\gamma_1 = 1$): **a** displacement, **b** impact force, **c** friction force

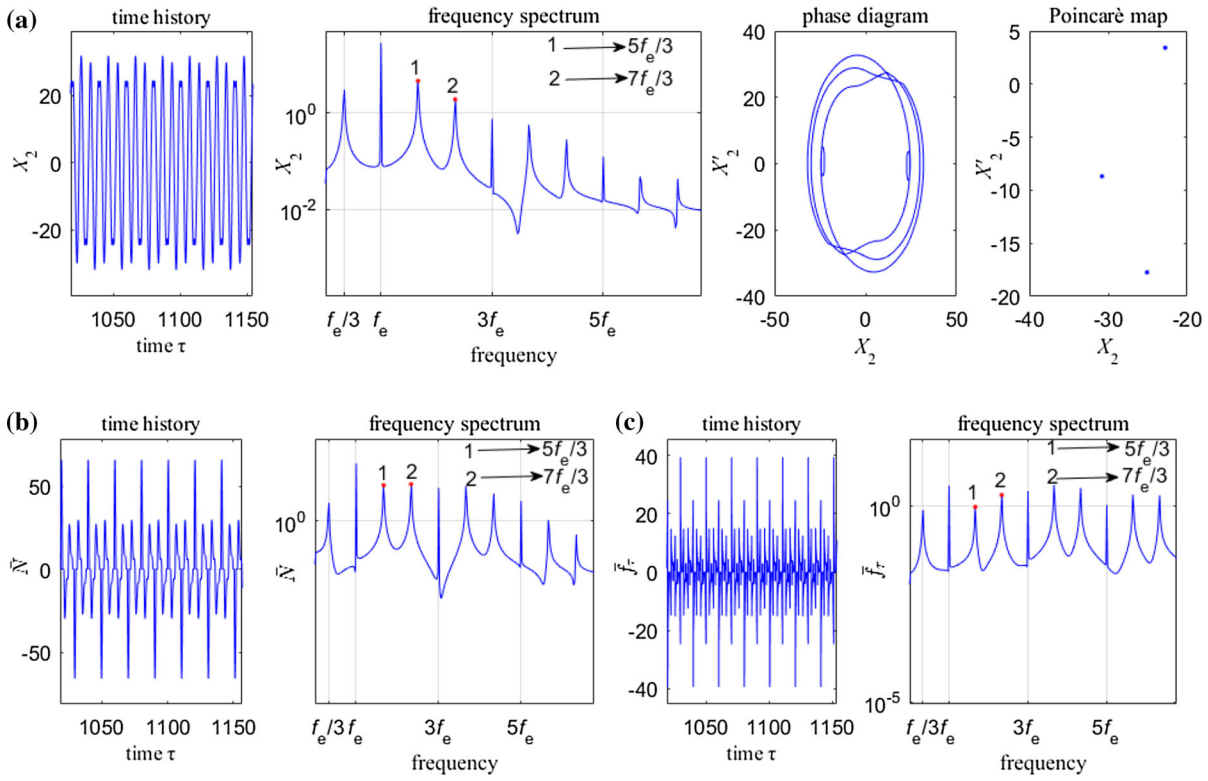

Fig. 8 Vibration responses of the reference blade ($\gamma_1 = 3.5$): **a** displacement, **b** impact force, **c** friction force

$$\bar{f}_{\tau 2} = \frac{-1}{3\cos\alpha}\left(\bar{Q}_1 + \bar{Q}_2 - 2\bar{Q}_3 + 3\bar{N}_2\sin\alpha - \mathrm{C}_1 - 2\,\mathrm{C}_2\right) \tag{22}$$

In Eqs. (15–22), C_1 is the horizontal displacement difference between the left shroud and the reference shroud at the end of the previous slip phase and C_2 is the horizontal displacement difference between the reference shroud and the right shroud at the end of the previous slip phase.

It should now be clear that during vibration the surfaces in contact stick or slip between each other and separate from each other. This is a very complicated nonsmooth dynamic process.

A numerical integration scheme implementing Runge–Kutta algorithm appropriate for the second-order differential equations coded in MATLAB and capable of dealing with nonsmooth friction and contact behaviour is developed to solve the equations of motion of the shrouded blades in different motion stages in this paper. The precise time instants when stick regime switches to slip regime and the precise time instants of separation and reconnection must be captured, and vice versa; the bisection method is used to find the critical points where the dynamics switches from one phase to another phase.

3 Numerical simulation

As an example, the material constants and geometric parameters of the blades are taken as: Young modulus $E = 2.1 \times 10^{11}$ Pa, mass density $\rho = 7800\,\mathrm{kg/m^3}$, length of the blade $L = 0.15\,\mathrm{m}$, width of the blade $b = 0.05\,\mathrm{m}$, thickness of the blade $h = 0.007\,\mathrm{m}$, viscous damping coefficient $c = 4\,\mathrm{Ns/m}$, and mass of the blade shroud $m = 0.082\,\mathrm{kg}$, the dynamic stiffness $k = m\,(2\pi f_{\mathrm{d1}})^2$, $\mu_{\mathrm{s}} = 0.5$, $\mu_{\mathrm{m}} = 0.3$, $\beta = 5\,\mathrm{s/m}$.

3.1 Vibration response analysis of shrouded blade with rubbing-impact

In this section, the effects of stiffness ratio, rotating speed and aerodynamic excitation amplitude on the vibration responses of integrally shrouded group blades

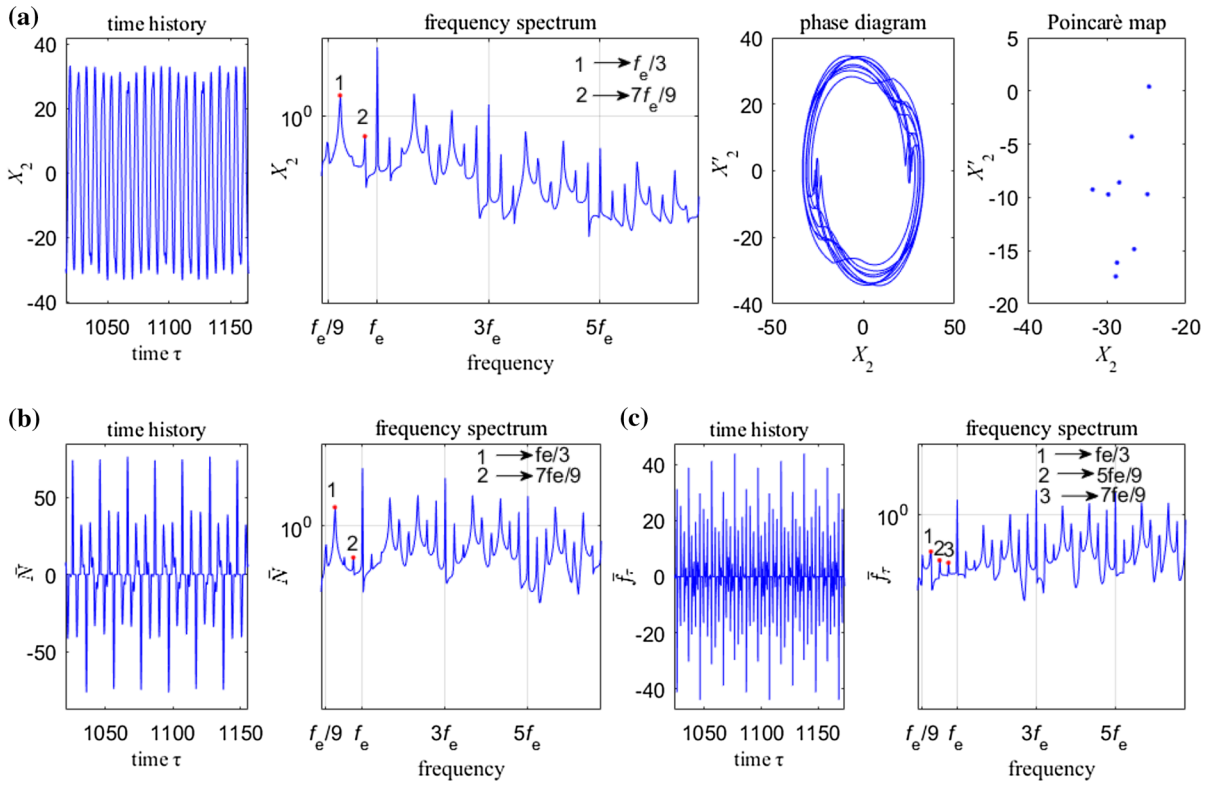

Fig. 9 Vibration responses of the reference blade ($\gamma_1 = 5.31$): **a** displacement, **b** impact force, **c** friction force

are discussed. $\Delta_1 = \Delta_2 = 0.02$ mm, $\alpha = \frac{\pi}{3}$ are taken for this study.

3.1.1 The effect of stiffness ratio γ_1 on vibration responses

The effect of stiffness ratio on the vibration responses of integrally shrouded group blades is investigated. The bifurcation diagram of the reference blade versus stiffness ratio γ_1 is shown in Fig. 6. Chaos occurs in certain stiffness ratio bands which are separated by bands with p-periodic motions of order $p = 1, 3, 5, 9$. Vibration responses of the reference blade at $\gamma_1 = 1,\ 3.5,\ 5.31,\ 6,\ 8.8$ are given in Figs. 7, 8, 9, 10 and 11, respectively. Period-one (p1) motion of the reference blade appears at $\gamma_1 = 1$ (see Fig. 7). It can be seen from Fig. 7 that the forced vibration of the reference blade is periodic and has the same frequency as the excitation frequency and odd-order superharmonic frequencies of the driving frequency can be observed. Period-three (p3) motion, period-nine (p9) motion and period-five (p5) motion of the reference blade appear at $\gamma_1 = 3.5,\ 5.31,\ 8.8$ are illustrated in Figs. 8, 9 and 11, respectively. Some fractional frequencies and some odd multiple frequencies $3f_e$ and $5f_e$ can be found from Figs. 8, 9 and 11. The reason for p3 motion at $\gamma_1 = 3.5$ is that there exists a rubbing-impact period which is three times of the excitation period, and the reasons for p5 motion and p9 motion are similar to p3 motion. Figure 10 displays the chaotic motion of the reference blade, where continuous spectrums appear.

3.1.2 The effect of rotating speed Ω on vibration responses

The effect of rotating speed on the vibration responses of integrally shrouded group blades is studied. Figure 12 shows bifurcation diagram of the reference blade versus rotating speed Ω. Period-one (p1) motion, period-three (p3) motion and quasi-periodic motion of the reference blade can be found from Fig. 12. Vibration responses of the reference blade at different rotating speeds are provided in Figs. 13, 14 and 15. Figure 13

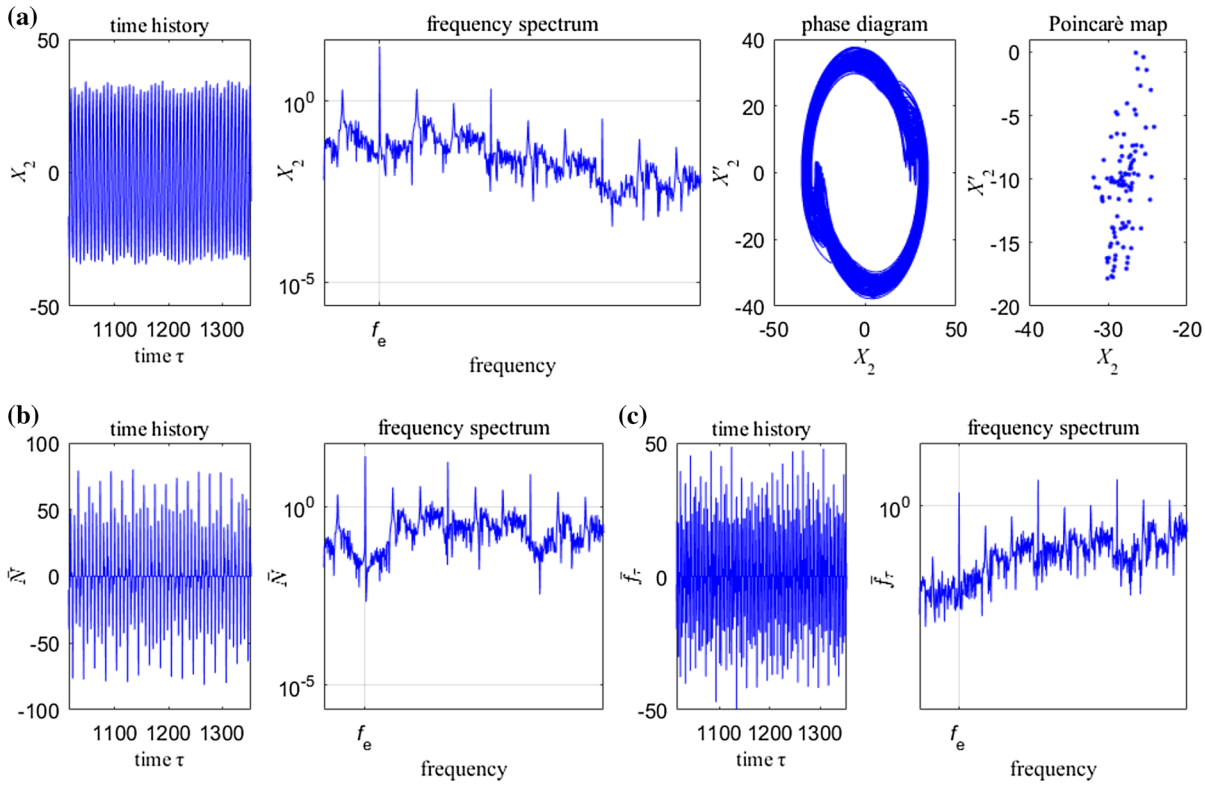

Fig. 10 Vibration responses of the reference blade ($\gamma_1 = 6$): **a** displacement, **b** impact force, **c** friction force

illustrates the period-one (p1) motion which appears at $\Omega = 5030\,\text{rev/min}$ of the reference blade. Excitation frequency f_e and only some odd multiple frequencies $3f_e$ and $5f_e$ can be observed, thus vibration response of the reference blade is periodic whose period is the period of excitation. Period-three (p3) motion of the reference blade appears at $\Omega = 5790\,\text{rev/min}$ and is shown in Fig. 14. Some fractional frequencies $f_e/3$, $5f_e/3$ and $7f_e/3$ and some odd multiple frequencies $3f_e$ and $5f_e$ can be found (see Fig. 14). Figure 15 displays the quasi-periodic motion of the reference blade which appears at $\Omega = 5990\,\text{rev/min}$. The Poincarè map of the reference blade is now a closed curve and there are several peaks in the frequency spectrums (see Fig. 15).

3.1.3 The effect of aerodynamic excitation amplitude q_1 on vibration responses

This subsection investigates the effect of aerodynamic excitation amplitude on the vibration responses of integrally shrouded group blades. Bifurcation diagram of the reference blade versus aerodynamic excitation amplitude q_1 is given in Fig. 16. With the increase in q_1, the motion of the reference blade changes from period-one motion to period-three (p3) motion at first, then changes to quasi-periodic motion, at last changes to period-three (p3) motion. Vibration responses of the reference blade at $q_1 = 5\,\text{N}$, 20N, 50 N are given in Figs. 17, 18 and 19, respectively. Figure 17 shows the period-one (p1) motion of the reference blade which appears at $q_1 = 5\,\text{N}$. Phase diagram of the reference blade is a closed curve, and there is only one point on the Poincarè map of the reference blade (see Fig. 17a). Excitation frequency f_e and only some odd multiple frequencies $3f_e$ and $5f_e$ can be observed as well. Period-three (p3) motion of the reference blade appears at $q_1 = 20\,\text{N}$ and is illustrated in Fig. 18. Some fractional frequencies $f_e/3, 5f_e/3$ and $7f_e/3$ and some odd multiple frequencies $3f_e$ and $5f_e$ can be found and the point number of the Poincarè map of the reference blade is now changed to three in comparison with the

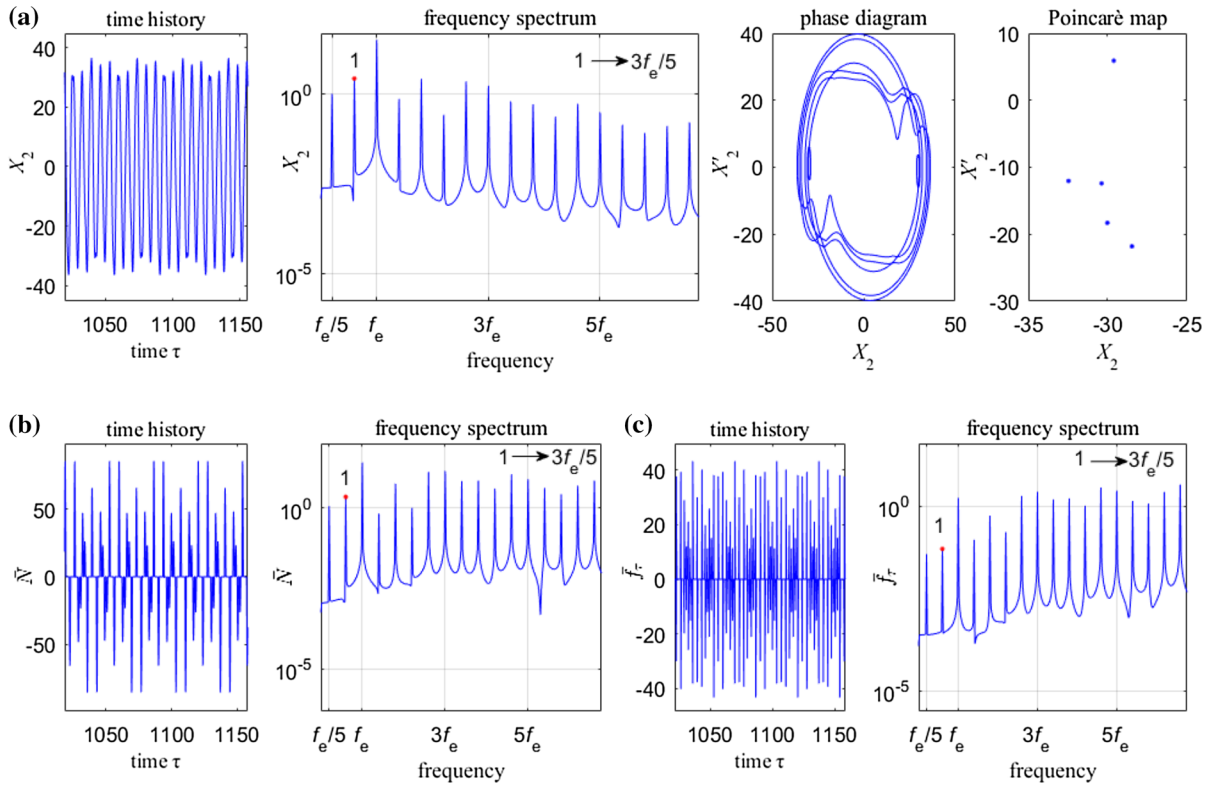

Fig. 11 Vibration responses of the reference blade ($\gamma_1 = 8.8$): **a** displacement, **b** impact force, **c** friction force

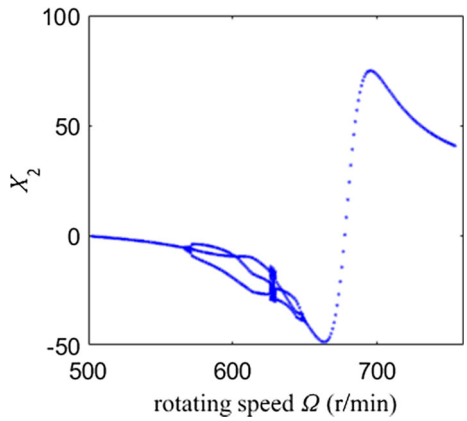

Fig. 12 Bifurcation diagram of the reference blade versus rotating speed Ω ($\gamma_1 = 2.2, q_1 = 50\,\mathrm{N}$)

p1 motion (see Fig. 18). The quasi-periodic motion of the reference blade appears at $q_1 = 50\,\mathrm{N}$. The Poincarè map of the reference blade is now a closed curve and the phase diagram is a closed ring, more peaks in the frequency spectrums can be found.

3.2 Energy dissipation study

In order to predict the effect of some key parameters on the blade vibration reduction, a normalised energy density (E_ρ) is defined below as a measure of vibration response so that the vibration reduction effect of the shroud in various conditions can be assessed. The smallest E_ρ is considered to indicate the best vibration reduction. $E_\rho = (\int_{t_1}^{t_2} x_2\,(t)^2\,\mathrm{d}t)/\,(t_2 - t_1)$. The interval (t_1, t_2) should be chosen after the response becomes "steady" and the value of $(t_2 - t_1)$ should be greater than the "steady" response period. In this section, the resonance frequency is selected, which corresponds to the crossing point between the first flexural dynamic frequency $f_{\mathrm{d}1}$ and aerodynamic excitation frequency f_e (see Fig. 20). The numerical simulation parameters are selected as $q_1 = 25\,\mathrm{N}$, $K = 1$, $\Omega = 6847.5\,\mathrm{rev/min}$, $f_\mathrm{e} = 216.25\,\mathrm{Hz}$, $\eta = 0.5$. The effects of stiffness ratio, initial gap, contact angle for vibration reduction are investigated.

The normalised energy density versus stiffness ratio curves at different initial gaps are illustrated in Fig. 21.

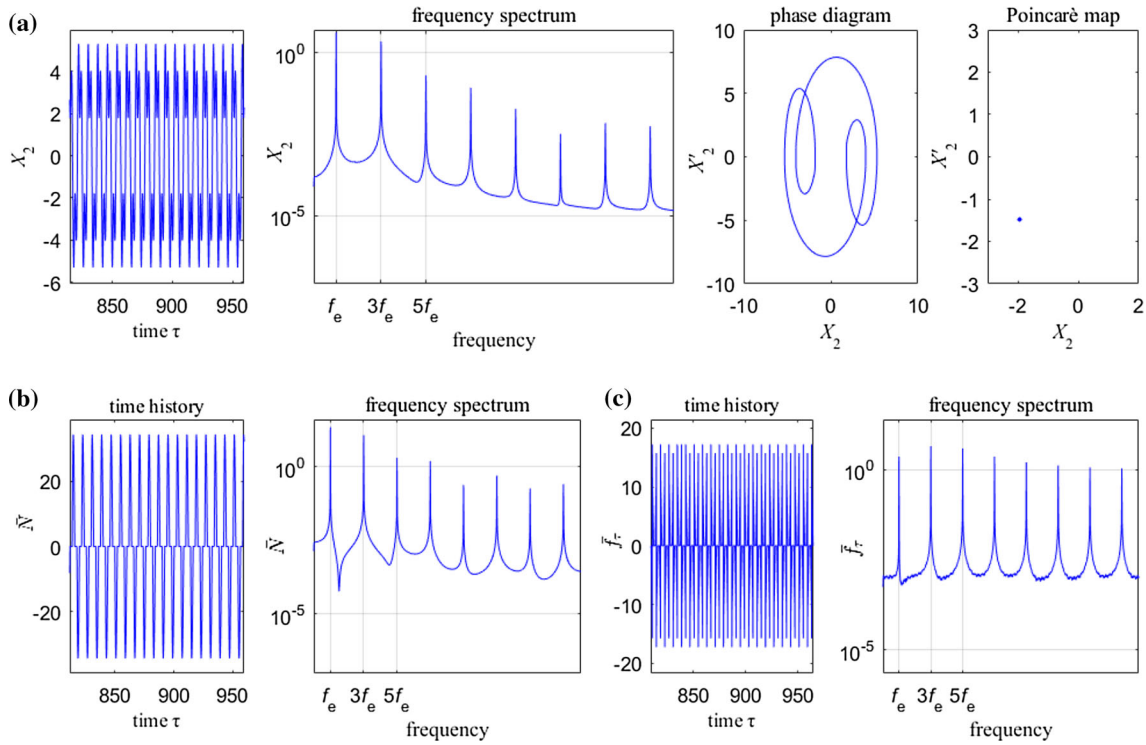

Fig. 13 Vibration responses of the reference blade ($\Omega = 5030$ rev/min): **a** displacement, **b** impact force, **c** friction force

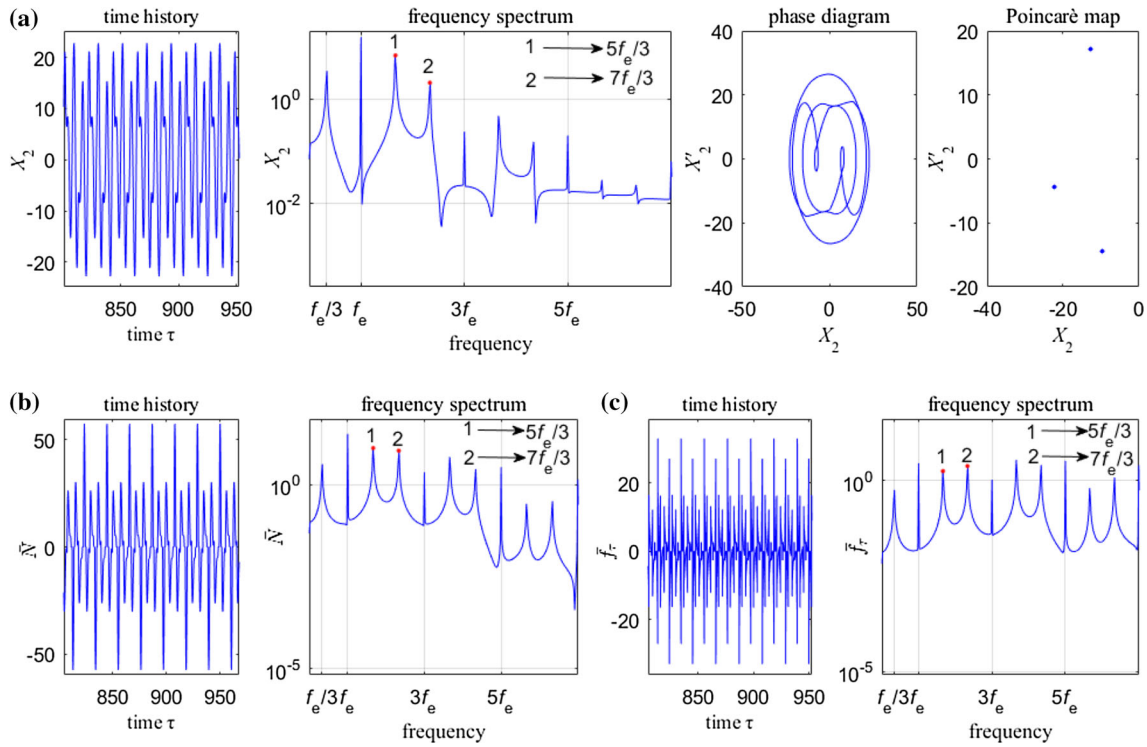

Fig. 14 Vibration responses of the reference blade ($\Omega = 5790$ rev/min): **a** displacement, **b** impact force, **c** friction force

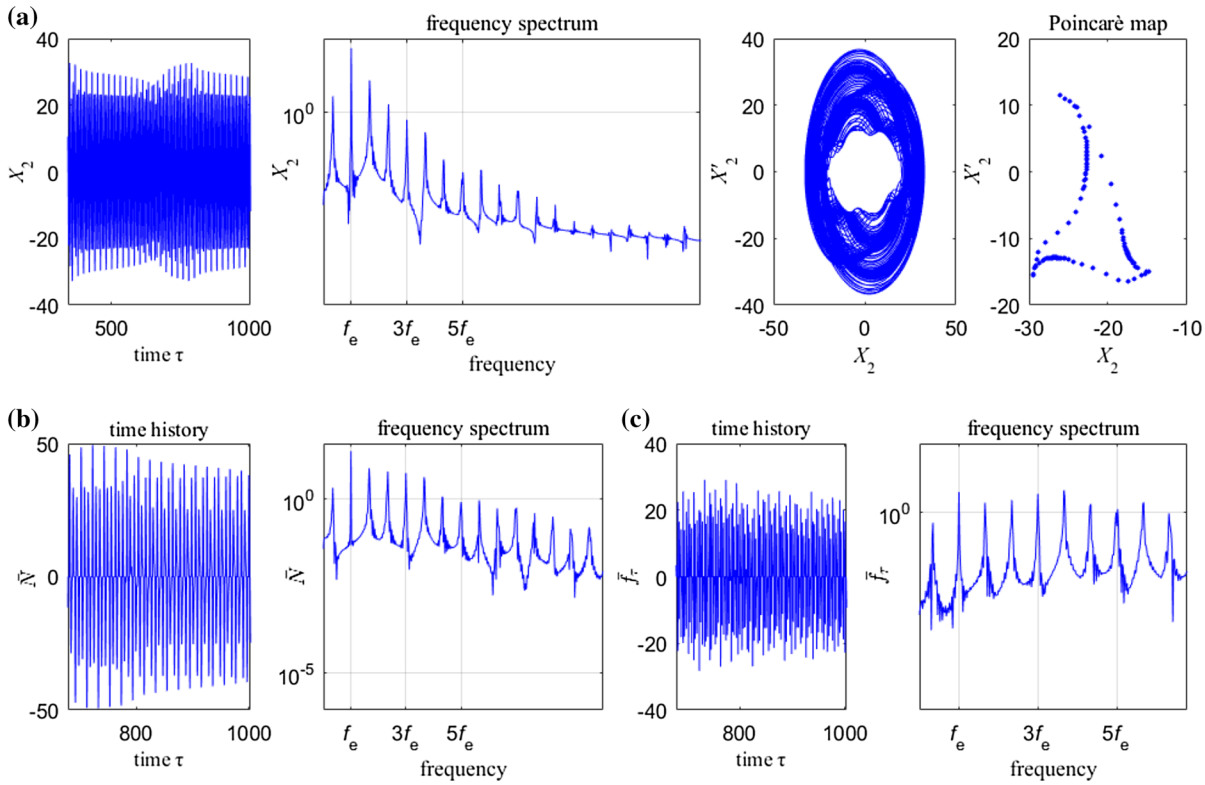

Fig. 15 Vibration responses of the reference blade ($\Omega = 5990$ rev/min): **a** displacement, **b** impact force, **c** friction force

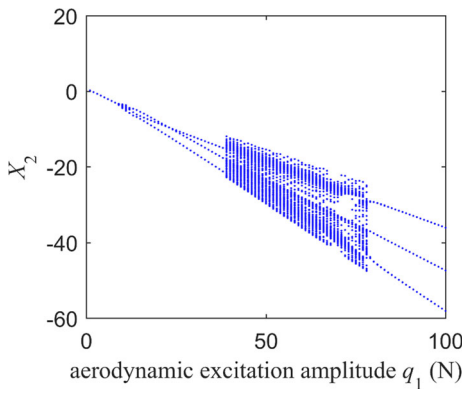

Fig. 16 Bifurcation diagram of the reference blade versus aerodynamic excitation amplitude q_1 ($\gamma_1 = 2.2$, $\Omega = 6000$ rev/min)

With the increase in stiffness ratio γ_1, the normalised energy density (E_ρ) decreases continuously at first, then stays the same. When the initial gap Δ_1 is relatively large, the stiffness ratio has a great effect on the normalised energy density; however, when $\Delta_1 < 0.02$ mm, the stiffness ratio has almost no influence on the normalised energy density. Figure 22 shows the normalised energy density versus the initial gap curves. It can be seen from Fig. 22 that when $\Delta_1 < 0.0074$ m impact between adjacent shrouded blades appears, and the normalised energy density increases with the increase in the initial gap; thus the smaller the initial gap, the better the damping effect. The normalised energy density versus the contact angle curves at $\Delta_1 = 0.02$ mm are given in Fig. 23. The normalised energy density E_ρ decreases continuously at first, then increases (see Fig. 23), so there is an intermediate range of the contact angle α which can make the best vibration reduction at $\Delta_1 = 0.02$ mm. This finding can be exploited to design shrouds that give the best vibration effect.

4 Conclusions

This paper presents a study on the forced vibration responses of integrally shrouded group blades with rubbing and impact. A lumped mass model of inte-

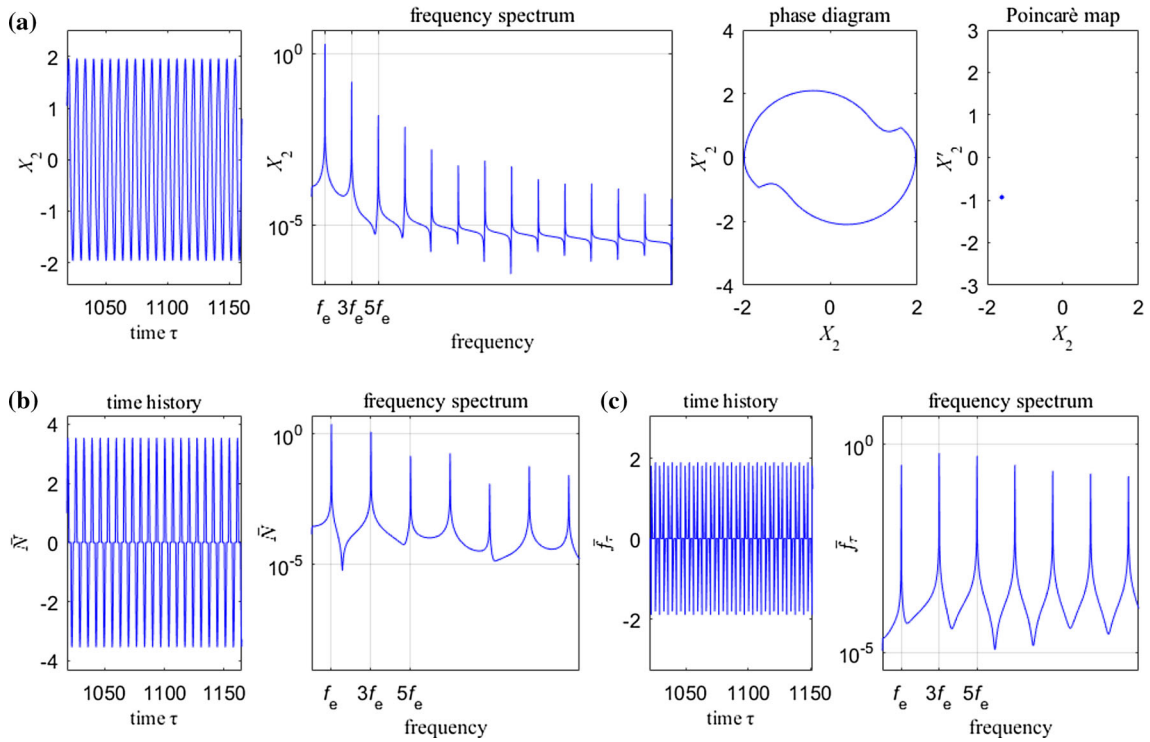

Fig. 17 Vibration responses of the reference blade ($q_1 = 5$ N): **a** displacement, **b** impact force, **c** friction force

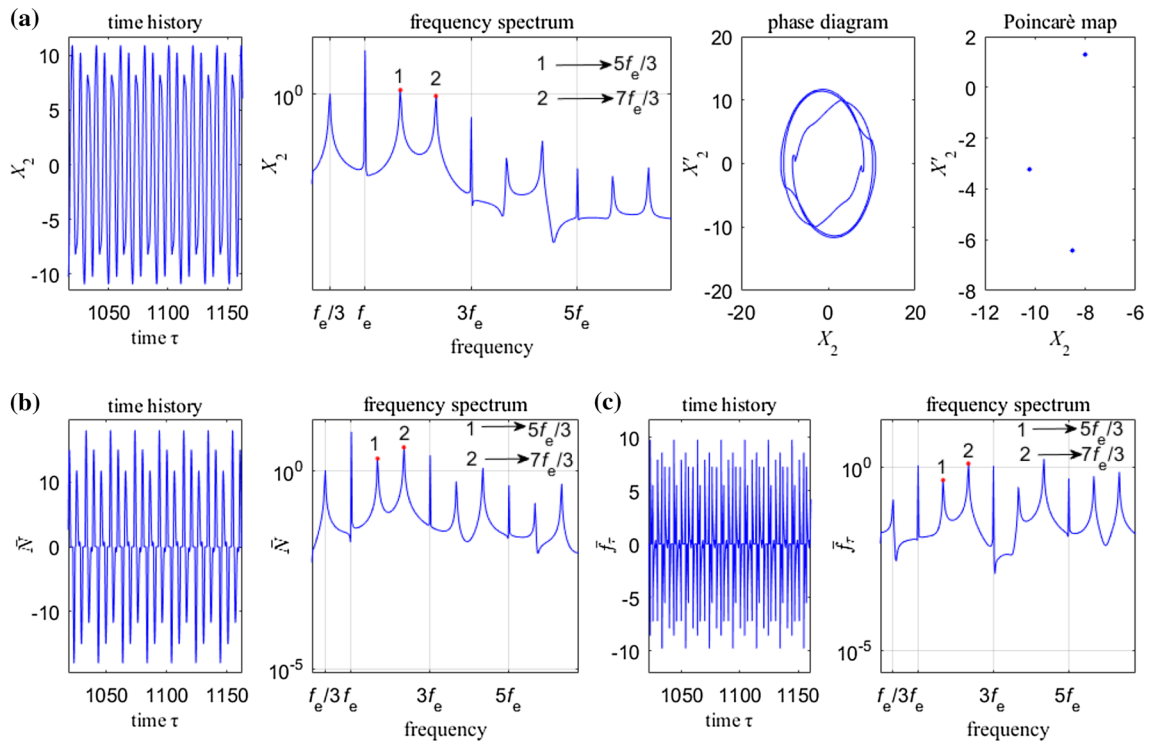

Fig. 18 Vibration responses of the reference blade ($q_1 = 20$ N): **a** displacement, **b** impact force, **c** friction force

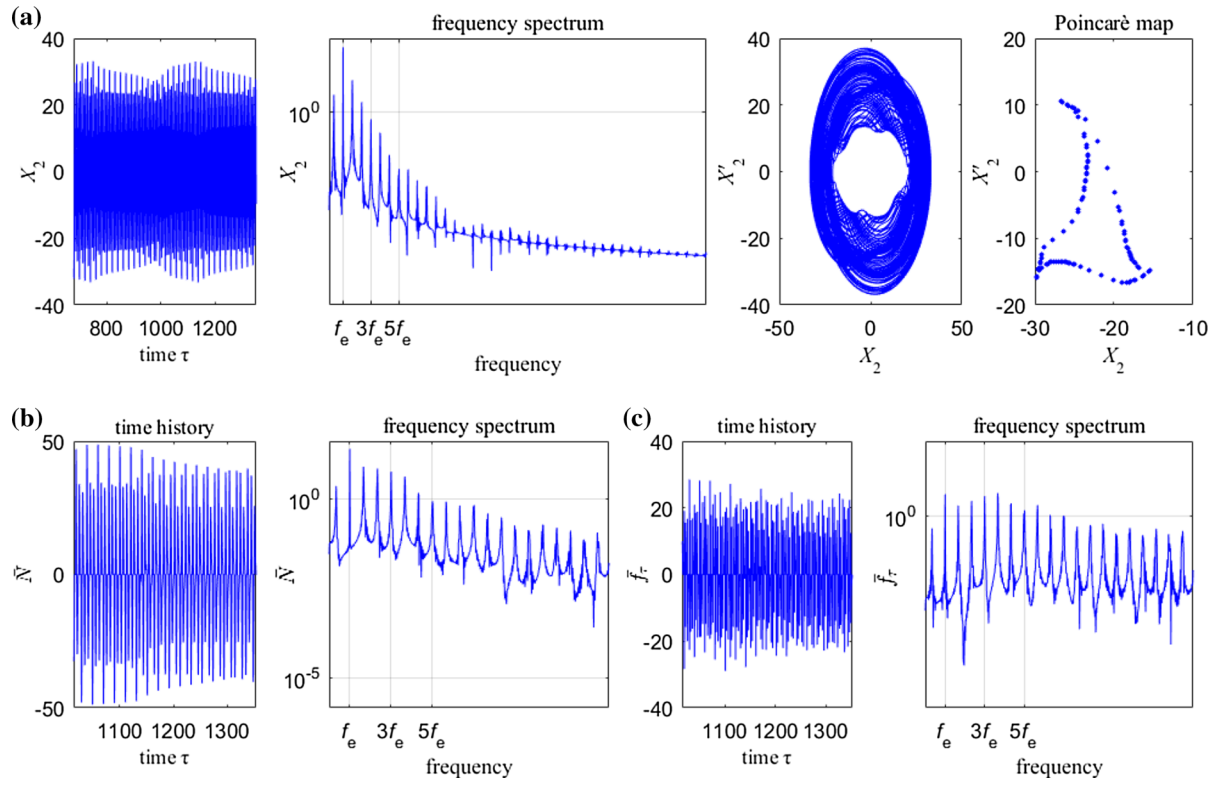

Fig. 19 Vibration responses of the reference blade ($q_1 = 50\,\mathrm{N}$): **a** displacement, **b** impact force, **c** friction force

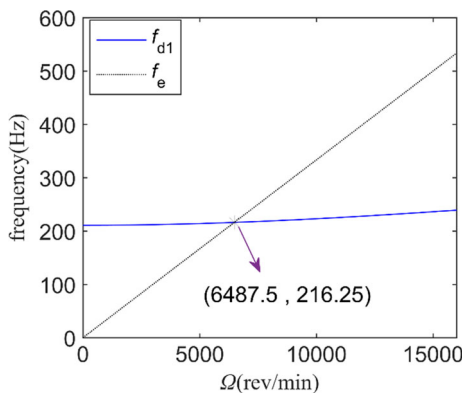

Fig. 20 Campbell diagram of the rotating shrouded blade

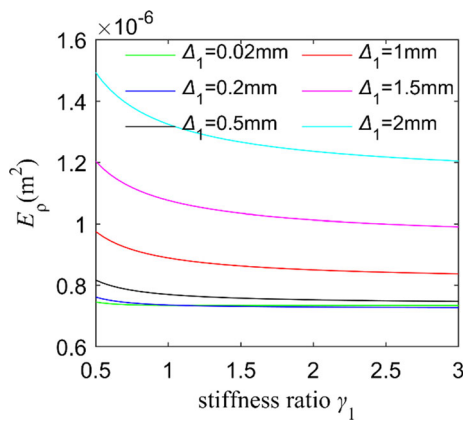

Fig. 21 Normalised energy density versus stiffness ratio γ_1 curve ($\alpha = \frac{\pi}{3}$)

grally shrouded group blades is established. This model displays nonsmooth and nonlinear dynamic behaviour and there are several distinct dynamic regimes, which present numerical difficulties. Using this model, the effects of stiffness ratio, rotating speed and excitation amplitude on the vibration characteristics of integrally shrouded group blades are analysed, and vibration reduction effect of the shroud at first dynamic resonance speed of the reference blade is demonstrated. The following conclusions can be drawn:

1. The reference blade could experience period-one motion, period-three motion, period-five motion,

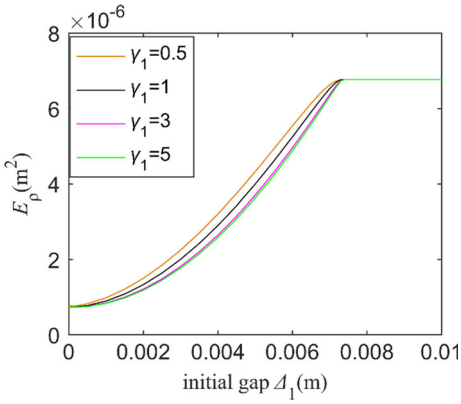

Fig. 22 Normalised energy density versus initial gap Δ_1 curve ($\alpha = \frac{\pi}{3}$)

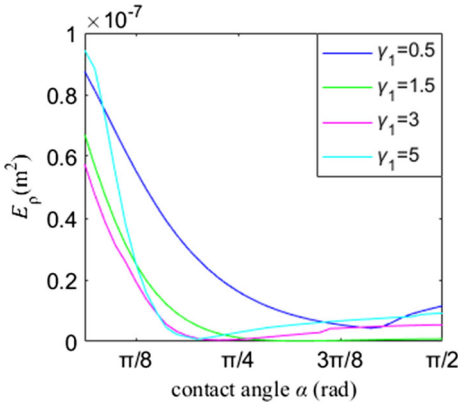

Fig. 23 Normalised energy density versus contact angle α curves ($\Delta_1 = 0.02$ mm)

period-nine motion and chaotic motion with the variation of the stiffness ratio γ_1.

2. Period-one motion, period-three motion and quasi-periodic motion of the reference blade can be found as the rotating speed Ω increases.
3. With the increase in excitation amplitude q_1, the motion of the reference blade changes from period-one motion to period-three motion at first, then changes to quasi-periodic motion, at last changes to period-three motion again.
4. With the increase in stiffness ratio γ_1, the normalised energy density (E_ρ) decreases continuously at first, then stays the same. When the initial gap Δ_1 is relatively large, the stiffness ratio has a great effect on the normalised energy density, however, when Δ_1 is less than a certain value (for instance, 0.02 mm in this investigation), the stiffness ratio has almost no influence on the normalised energy density. Contact between adjacent shrouded blades appears when Δ_1 is less than a certain value (for example, 0.0074 m in this investigation). When Δ_1 is less than a certain value (for example, 0.0074 m in this investigation), the normalised energy density increases with the increase in the initial gap. The normalised energy density E_ρ decreases continuously at first, and then increases as contact angle α increases.

Acknowledgements The authors are grateful to the support by the National Natural Science Foundation of China (Grant No. 11672052 and No. 51405452), and Foundation of He'nan Educational Committee (Grant No. 15A130002).

References

1. Bhaumik, S., Sujata, M., Venkataswamy, M., Parameswara, M.: Failure of a low pressure turbine rotor blade of an aero-engine. Eng. Fail. Anal. **13**(8), 1202–1219 (2006)
2. Carter, T.J.: Common failures in gas turbine blades. Eng. Fail. Anal. **12**(2), 237–247 (2005)
3. Xie, Y., Meng, Q.: Numerical model for steam turbine blade fatigue life. J. Xian Jiaotong Univ. **36**(9), 912–915 (2002)
4. Wang, L., Li, J., Jiang, A., Jing, H.: Steady-state Solution of integrally shrouded group blades contact and impact system based on harmonic balance method. Turbine Technol. **56**(4), 246–248 (2014). (in Chinese)
5. Xu, Z., Xie, H., Park, J.P., Ryu, S.J.: Three-dimensional numerical simulation and experimental study on vibratory modes of group blades. J. Xi'an Jiaotong Univ. **24**(4), 385–396 (2003). (in Chinese)
6. Chiu, Y.J., Chen, D.Z., Yang, C.H.: Influence on coupling vibration of rotor system with grouped blades due to mis-tuned lacing wire. Appl. Mech. Mater. **101–102**, 1119–1125 (2012)
7. Tsai, G.C.: Rotating vibration behavior of the turbine blades with different groups of blades. J. Sound Vib. **271**(3), 547–575 (2004)
8. Allara, M.: A model for the characterization of friction contacts in turbine blades. J. Sound Vib. **320**(3), 527–544 (2009)
9. Popp, K., Panning, L., Sextro, W.: Vibration damping by friction forces: theory and applications. J. Vib. Control **9**(3–4), 419–448 (2003)
10. Chen, J., Menq, C.: Prediction of periodic response of blades having 3D nonlinear shroud constraints. In: ASME 1999 International Gas Turbine and Aeroengine Congress and Exhibition. American Society of Mechanical Engineers, pp. V004T003A033 (1999)
11. He, S., Ren, X., Nan, G.: One new method for analysing systems with dry friction damping. J. Mech. Strength **33**(1), 29–33 (2011)
12. Iwan, W.D.: The Dynamic Response of Bilinear Hysteretic Systems. California Institute of Technology, Pasadena (1961)

13. Hao, Y., Zhu, Z.: New method to resolve vibratory response of blades with friction damping. Acta Aeronaut. Astronaut. Sin. Ser. A B **22**(5), 411–414 (2001)
14. Yang, B., Menq, C.: Characterization of 3D contact kinematics and prediction of resonant response of structures having 3D frictional constraint. J. Sound Vib. **217**(5), 909–925 (1998)
15. Zhu, Z., Shan, Y.: The solution of nonlinear friction forces when friction interfaces constrained to complex contact motions. Lubr. Eng. **3**, 73–77 (2006). (in Chinese)
16. Zucca, S., Gola, M.M., Piraccini, F.: Non-linear dynamics of steam turbine blades with shroud: numerical analysis and experiments. In: ASME Turbo Expo: Turbine Technical Conference and Exposition, 2012. American Society of Mechanical Engineers, pp. 665–674 (2012)
17. Krack, M., Panning-von Scheidt, L., Wallaschek, J., Siewert, C., Hartung, A.: Reduced order modeling based on complex nonlinear modal analysis and its application to bladed disks with shroud contact. J. Eng. Gas Turbines Power **135**(10), 102502 (2013)
18. Pešek, L., Hajžman, M., Půst, L., Zeman, V., Byrtus, M., Brůha, J.: Experimental and numerical investigation of friction element dissipative effects in blade shrouding. Nonlinear Dyn. **79**(3), 1711–1726 (2015)
19. Ding, Q., Chen, Y.: Analyzing resonant response of a system with dry friction damper using an analytical method. J. Vib. Control **14**(8), 1111–1123 (2008)
20. Nan, G., Ren, X., He, S., Yang, Y.: Damped vibration characteristics of blades with tips of an aero-engine. J. Vib. Shock **28**(7), 135–138 (2009)
21. Iwan, W.D.: On a class of models for the yielding behavior of continuous and composite systems. J. Appl. Mech. **34**(3), 612 (1967)
22. Menq, C.-H., Bielak, J., Griffin, J.: The influence of microslip on vibratory response, part I: a new microslip model. J. Sound Vib. **107**(2), 279–293 (1986)
23. Menq, C.-H., Griffin, J., Bielak, J.: The influence of microslip on vibratory response. Part II: A comparison with experimental results. J. Sound Vib. **107**(2), 295–307 (1986)
24. Sanliturk, K., Ewins, D.: Modelling two-dimensional friction contact and its application using harmonic balance method. J. Sound Vib. **193**(2), 511–523 (1996)
25. Cigeroglu, E., An, N., Menq, C.-H.: A microslip friction model with normal load variation induced by normal motion. Nonlinear Dyn. **50**(3), 609–626 (2007)
26. Dubowsky, S., Freudenstein, F.: Dynamic analysis of mechanical systems with clearances 1. Part 1: Formation of dynamic model. J. Eng. Ind. **93**(1), 305–309 (1971)
27. Chu, S., Cao, D., Sun, S., Pan, J., Wang, L.: Impact vibration characteristics of a shrouded blade with asymmetric gaps under wake flow excitations. Nonlinear Dyn. **72**(3), 539–554 (2013)
28. Nan, G.: Modeling and dynamic analysis of shrouded turbine blades in aero-engines. J. Aerosp. Eng. **29**(1), 04015021 (2015)
29. Huang, B.: Effect of number of blades and distribution of cracks on vibration localization in a cracked pre-twisted blade system. Int. J. Mech. Sci. **48**(1), 1–10 (2006)
30. Lim, H.S., Yoo, H.H.: Dynamic Impact analysis of a rotating beam having a tip mass. Key Eng. Mater. **321–323**, 1649–1653 (2006)
31. Jeffers, T., Kielb, J., Abhari, R.: A novel technique for measurement of rotating blade damping. ASME Paper (2000-GT):359 (2000)
32. Ma, H., Xie, F., Nai, H., Wen, B.: Vibration characteristics analysis of rotating shrouded blades with impacts. J. Sound Vib. **378**, 92–108 (2016)
33. Liu, Y., Shangguan, B., Xu, Z.: A friction contact stiffness model of fractal geometry in forced response analysis of a shrouded blade. Nonlinear Dyn. **70**(3), 2247–2257 (2012)
34. Petrov, E.P., Ewins, D.J.: State-of-the-art dynamic analysis for non-linear gas turbine structures. Proc. Inst. Mech. Eng. Part G J. Aerosp. Eng. **218**(3), 199–211 (2004)
35. Santhosh, B., Narayanan, S., Padmanabhan, C.: Nonlinear dynamics of shrouded turbine blade system with impact and friction. Appl. Mech. Mater. **706**, 81–92 (2014)
36. Cao, D., Gong, X., Wei, D., Chu, S., Wang, L.: Nonlinear vibration characteristics of a flexible blade with friction damping due to tip-rub. Shock Vib. **18**(1–2), 105–114 (2011)
37. Dubowsky, S., Deck, J., Costello, H.: The dynamic modeling of flexible spatial machine systems with clearance connections. J. Mech. Transm. Autom. Des. **109**(1), 87–94 (1987)
38. Berger, E.: Friction modeling for dynamic system simulation. Appl. Mech. Rev. **55**(6), 535–577 (2002)